Towards Solving the PFAS Problem: The Potential Role of Metal-Organic Frameworks
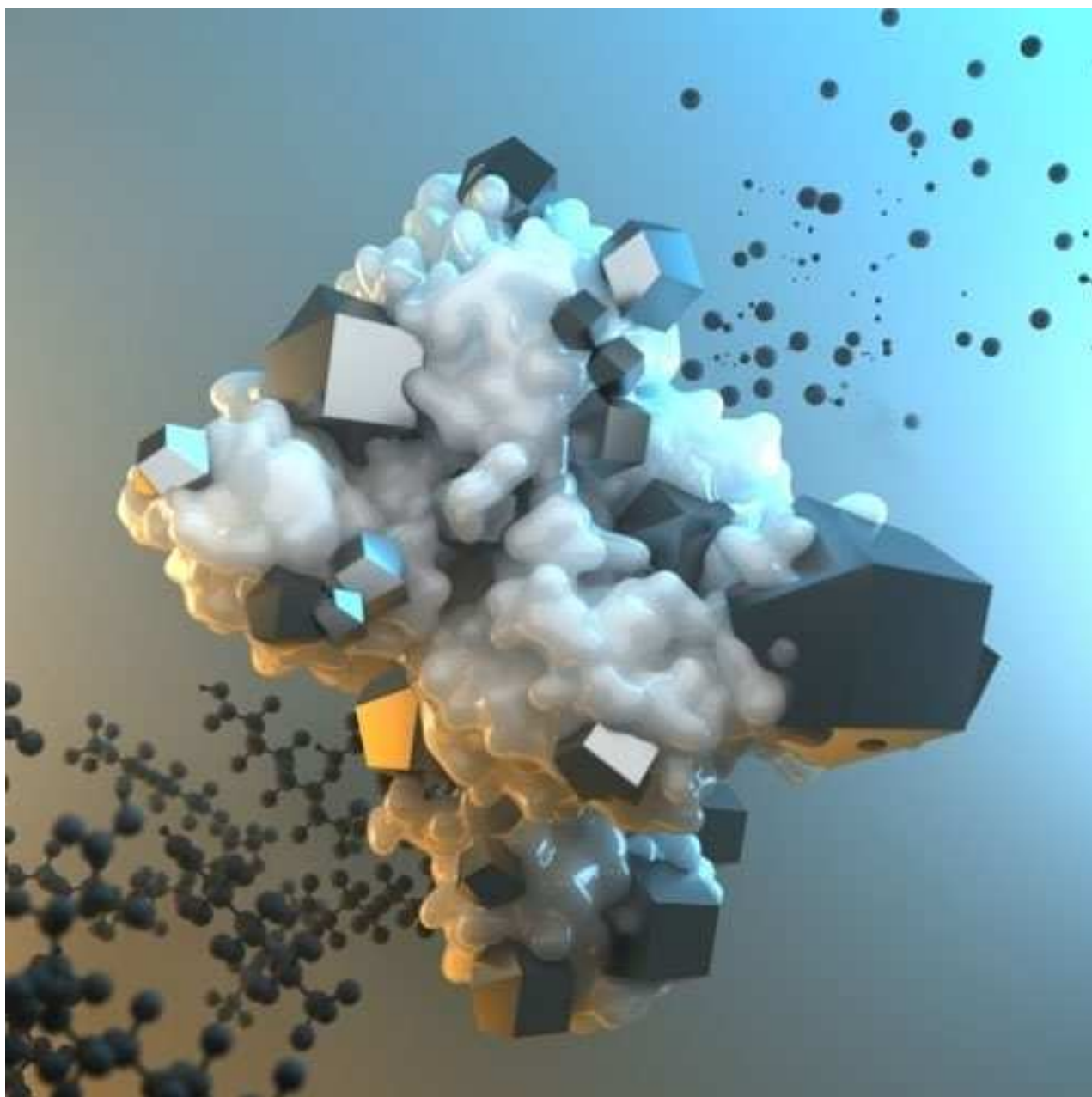
Laura I. FitzGerald,[a] Joseph F. Olorunyomi,[a] Ruhani Singh,[a] and Cara M. Doherty*[a]

Per- and polyfluoroalkyl substances (PFAS) are a group of recalcitrant molecules that have been used since the 1940s in a variety of applications. They are now linked to a host of negative health outcomes and are extremely resistant to degradation under environmental conditions. Currently, membrane technologies or adsorbents are used to remediate contaminated water. These techniques are either inefficient at capturing smaller PFAS molecules, have high energy demands, or result in concentrated waste that must be incinerated at high temperatures. This Review focuses on what role metal-organic frameworks (MOFs) may play in addressing the PFAS problem. Specifically, how the unique properties of MOFs such as their well-defined pore sizes, ultra-high internal surface area, and tunable surface chemistry may be a sustainable solution for PFAS contamination.

1. Introduction

There is increasing concern surrounding the health impacts of per- and polyfluoroalkyl substances (PFAS). These are a collection of synthetic molecules that contain at least one perfluoroalkyl moiety (C_nF_{2n+1}).[1] They have been used for decades in a variety of applications such as non-stick cookware, water-resistant clothing, and fire-fighting foams.[2] The desirable chemical properties that make them useful molecules also allow them to leach from soil into groundwater that can spread far from the initial contamination site, impacting farmland and drinking supplies. They have extremely high thermal and chemical stability due to the strength of carbon-fluorine bonds (≈ 460.24 kJ mol^{-1}),[3,4] which makes these molecules tremendously difficult to break down.[3] As such, they persist in the environment, bioaccumulating in plants and animals. PFAS has been linked to a range of negative health outcomes including thyroid issues, developmental problems, immunotoxicity, and an increase in the incidence of tumors.[5]

Due to the widespread historical use of perfluorooctanoic acid (PFOA, Figure 1a) and perfluorooctanesulfonic acid (PFOS, Figure 1b), they are the most studied and commonly detected PFAS species. As such, a large proportion of the literature on the technology for remediation of PFAS contamination focuses on these. Many countries have now banned or heavily regulated their use. They are often referred to as "long-chain" PFAS due to the number of carbons in their backbone (≥ 6 for sulfonates or ≥ 7 for carboxylic acids). As replacements, shorter-chain homologues such as perfluorobutanesulfonic acid (PFBS, Figure 1c) and hexafluoropropylene oxide dimer acid (GenX, Figure 1d) were introduced. It was thought that these substitutes were less likely to bioaccumulate, but recent data shows they may be just as toxic and persistent in the environment as their predecessors.[6]

The surfactant properties of PFAS make them mobile in groundwater, spreading them far from the initial contamination site, and they are highly recalcitrant. This makes removing PFAS from the environment extremely challenging. While many physio-chemical approaches have been reported for PFAS capture and degradation, such as adsorption, hydrogen peroxide-catalyzed breakdown, electrochemical, photolytic, or sonochemical oxidation, these options tend to be energy- and cost-intensive and require specialized equipment, hence limiting their utilization.[7,8] Established methods include granular activated carbon (GAC), anion exchange resins (AIX), and membrane technologies (nanofiltration and reverse osmosis). The most common of these treatments is GAC, which removes PFAS via adsorption through electrostatic and hydrophobic interactions (Figure 1g). Anion exchange resins also adsorb PFAS and do so by reversibly swapping with ions on a solid resin (Figure 1f). In nanofiltration and reverse osmosis, contaminated water is subjected to a high pressure and pushed against a semi-permeable membrane, which traps PFAS based on size (Figure 1e).

All these systems can remove PFAS from water, each with their own advantages and disadvantages. Membrane technologies have been shown to be extremely effective at removing long-chain (90–99%) PFAS, but not as effective with the removal of short-chain PFAS (50–99%).[9] They are the most expensive to set up and operate as they require significant energy to generate the high pressures required. GAC and AIX are more cost effective but may be less efficient at removing PFAS, especially short-chain compounds. All the technologies require incineration of either a concentrated waste stream, a spent resin, or reactivation, which requires temperatures above 1100 °C.[10]

Metal-organic frameworks (MOF) are ordered porous crystalline solids with ultra-high internal surface areas.[11] They are formed via the coordination of linkers around metal nodes (Figure 1h). By selecting different metal centers for the organic linkers to coordinate around, internal surface properties and pore sizes can be tuned.[12] These attributes make them attractive for a variety of applications including separation, adsorption, catalysis, and sensing, so they have also been considered for the remediation of a variety of xenobiotic compounds including PFAS. Herein, the potential of MOFs as a sustainable approach in the remediation of PFAS-contaminated soil and water is discussed. We begin by covering how these porous materials can compete with currently used commercial adsorbents. We then move on to how MOFs can be used to breakdown PFAS through photo- and enzyme catalysis as well as emerging work on biodegradation by bacteria. Finally, we discuss the potential of MOFs in overcoming the shortcomings of traditional PFAS sensing.

[a] Dr. L. I. FitzGerald, Dr. J. F. Olorunyomi, Dr. R. Singh, Dr. C. M. Doherty
CSIRO Manufacturing
Private Bag 10, Clayton South 3169, Victoria (Australia)
E-mail: Cara.Doherty@csiro.au

ChemSusChem

Review
doi.org/10.1002/cssc.202201136

Chemistry Europe
European Chemical
Societies Publishing

2. Removal by Adsorption

The porosity and ultra-high surface areas of MOFs have led to them being considered for adsorption of a variety of pollutants, including PFAS. Cr- and Zr-based MOFs are the most studied families of MOFs for PFAS adsorption (Table 1). This is likely due to their high stability in water[14] over broad pH ranges as well as the possibility of strong electrostatic interactions between the anionic head of the PFAS molecules and the cationic inorganic nodes of these MOFs, which may contribute to their adsorption. A thorough comparison of the adsorption of PFAS by activated carbon and MOFs has recently been published elsewhere.[13]

The mesoporous chromium-based Materials Institute Lavoisier [MIL-101(Cr)] MOF has been demonstrated to adsorb both PFOA and PFOS. Liu et al. pre- and post-synthetically modified this MOF to contain amine functional groups in order to enhance adsorption of PFOA.[15] They showed that pristine MIL-101(Cr) has an adsorption capacity of 1.11 mmol g^{-1}, while pre-synthetically functionalizing with an amine decreased the adsorption to 0.7 mmol g^{-1} as this modification blocks entrance of PFOA to the internal pores. Post-synthetically introducing quaternary-ammonium groups, however, increased the adsorption up to 1.82 mmol g^{-1}. MIL-101 has also been demonstrated to adsorb PFOS in work by Barpaga et al. through scanning transmission electron microscopy energy-dispersive X-ray spectroscopy (STEM-EDS) and infrared (IR) spectroscopy data, but the adsorption capacity was not reported.[21] The concentrations used in this study (up to 100 mmol L^{-1}) were relatively high compared to upper health advisory limit set by the EPA at 70 ng L^{-1} for drinking water.[16] As the critical micelle concentration of PFOS is approximately 8 mmol L^{-1}, the amounts used in this study would form aggregates that would impact adsorption.[17]

Like MIL-101(Cr), UiO-66 is also formed with 1,4-benzenedicarboxylate but uses a zirconium center and has been shown to be promising for PFAS capture. Sini et al. synthesized both UiO-66 and its fluorinated version, UiO-66-(F4) and compared their ability to take up PFOA and PFOS from an aqueous solution. They demonstrated that both MOFs displayed fast adsorption kinetics (< 1 h equilibrium time) and had excellent capacity at adsorbing PFAS. They also showed the fluorinated MOF had higher capacity (1.13 mmol g^{-1} PFOA and 0.51 mmol g^{-1} PFOS) than non-fluorinated UiO-66 (0.94 mmol g^{-1} PFOA and 0.32 mmol g^{-1} PFOS). Binding was attributed to hydrophobic interactions of the PFAS molecules with the MOF rather than attraction to the metal node, which explained why the fluorinated MOF was more effective due to increased van der Waals interactions.[19]

Further work using UiO-66 engineered to contain defects was performed by Clark et al.[20] They synthesized UiO-66 using increasing amounts of hydrochloric acid (0–50 vol%) to induce crystal irregularities, which modified the surface area of the MOF.[23] They demonstrated that introducing larger pores drastically increased adsorption compared to the defect-free material (Figure 2a). They also showed it had around 2 times more capacity (1.24 mmol g^{-1}) than activated carbon (0.64 mmol g^{-1}) but lower adsorption capacity than the commercial anion exchange resin, IRA-900 (2.55 mmol g^{-1}) (Figure 2b). However, UiO-66 displayed superior kinetics and reached equilibrium within 60 min compared to 72 h for IRA-900. They also showed the PFOS substitute PFBS was adsorbed

Laura FitzGerald is a postdoctoral research fellow at CSIRO and is currently working on encapsulating biomolecules with metal-organic frameworks to enhance their stability. Prior to joining in 2021, she completed a Bachelor of Science (Chemistry) and Master of Engineering (Chemical) at the University of Melbourne before undertaking a Ph.D. in chemical biology at the Monash Institute of Pharmaceutical Sciences (MIPS). Her past research focused on designing fluorescent sensors to probe the interactions between nanomaterials and cells.

Joseph Olorunyomi received his Bachelor's and Master of Philosophy degrees in Chemistry from the Obafemi Awolowo University, Ile-Ife, Nigeria and the University of Hong Kong, Hong Kong, respectively. He recently completed his Ph.D. study at RMIT University, Australia under the joint supervision of Prof. Rachel Caruso (RMIT) and Dr Cara Doherty, CSIRO, Australia. His research focused on the development of metal-organic framework (MOF) composite materials for chemical detection using fluorescence techniques toward the development of MOF-based sensors.

Ruhani Singh has a Master of Engineering from the University of Melbourne and a Ph.D. in Chemistry and Pharmacology from the University of Western Australia. During her Ph.D., she worked on developing and validating theranostic nanoparticles in clinically relevant prostate cancer models. She then undertook a postdoctoral fellowship at CSIRO where her research focused on using coordination polymers for biomedical applications, in particular the encapsulation of live-viral and nucleic acid vaccines to enhance their thermal stability.

Cara Doherty is a materials scientist. She undertook her Ph.D. studies in Physical Chemistry at the University of Melbourne, developing porous electrode materials for lithium-ion batteries. She is presently a 'Veski Inspiring Women Fellow' and leading a research team at CSIRO developing advanced porous materials used for the benefit of the environment including sensors for toxic water systems, device fabrication and membranes for energy storage. Cara also specializes in Positron Annihilation Lifetime Spectroscopy (PALS) for the characterization of porous materials.
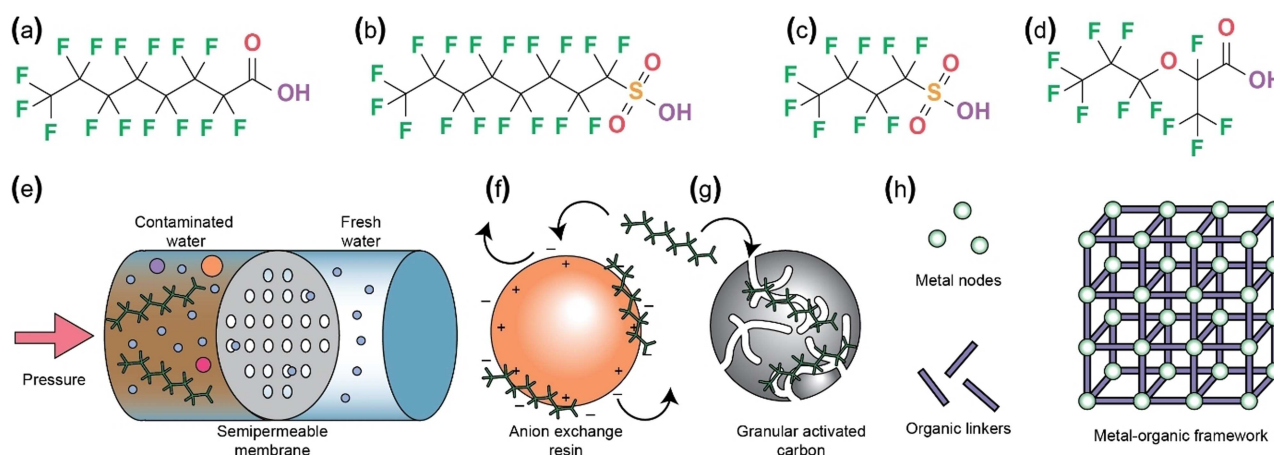
ChemSusChem

Review
doi.org/10.1002/cssc.202201136

Chemistry
Europe
European Chemical
Societies Publishing

Figure 1. Common PFAS molecules and present removal technologies. Previously used long-chain PFAS molecules (a) perfluorooctanoic acid (PFOA) and (b) perfluorooctanesulfonic acid (PFOS) are now being replaced with short-chain substitutes including (c) perfluorobutanesulfonic acid (PFBS) and (d) hexafluoropropylene oxide dimer acid (GenX). (e) Nanofiltration/reverse osmosis: contaminated water is subjected to high pressure against a semipermeable membrane and is filtered based on size. (f) Anion exchange resin: negatively charged PFAS is attracted to positive charges on synthetic polymeric resins are exchanged with ions. (g) Granular activated carbon: PFAS is adsorbed through electrostatic and hydrophobic effects. (h) Metal-organic frameworks are formed from the coordination of organic linkers around metal nodes to form ordered crystalline solids.

Table 1. MOFs for PFAS adsorption.

MOF	Adsorption capacity [mmol g^{-1}]	BET surface area [m^2 g^{-1}]	Concentration tested [mmol L^{-1}]	Type	Ref.
MIL-101(Cr)	1.11	2560	0.1–0.6	PFOA	[15]
ZIF-7	0.052	17	0.01–0.5	PFOA	[18]
ZIF-8	0.428	1291			
ZIF-L	0.589	12			
UiO-66	0.94 (PFOA)	682	0.2–2.4	PFOA/PFOS	[19]
UiO-66-(F4)	0.32 (PFOS) 1.13 (PFOA) 0.51 (PFOS)				
UiO-66	0.19–1.24	687–1423	1–1.7	PFOS/PFBS	[20]
MIL-101(Cr)	not reported	not reported	1–100	PFOS	[21]
NU-1000	1.22 (PFOA) 1.24 (PFOS)	2255	2.6×10^{-4} (PFOA) 8.5×10^{4} (PFOS)	various	[22]

with similar capacity and kinetics. The reason for the better adsorption capacity in the resin is likely due to the presence of cationic trimethylammonium group attached to the hydrocarbon chains of the resin, leading to higher electrostatic interaction with PFAS than with UiO-66. Hence, it may be possible to functionalize the MOF interior with ligands to also facilitate ionic bonds, which may improve performance.

The ability of another zirconium-based MOF, NU-1000, to capture a range of PFAS molecules has also been studied.[22] NU-1000 is formed from a 4,4′,4′′,4′′′-(pyrene-1,3,6,8-tetrayl)tetrabenzoic acid linker and a zirconyl chloride octahydrate precursor.[24] Li et al. demonstrated that the MOF NU-1000 could efficiently capture a range of PFSAs and PFCAs with different carbon chain lengths (1–9).[22] They showed most of the molecules tested were rapidly adsorbed where all except heptafluorobutyric acid (PFBA) reached equilibrium in under 1 min. The MOF showed high affinity for PFSAs where the capacity was shown to be 1.24 mmol g^{-1} while up to 1.55 mmol g^{-1} was retained for PFCAs, which was much higher than commercially available GAC or resin for this species. In

addition to showing that MOF NU-1000 could be regenerated with a 30:70% mixture of 0.1 M HCl in methanol, it also displayed 80–100% removal of PFAS from real groundwater samples collected from contaminated sites (Figure 2c).

These reports demonstrate that MOFs can be effective adsorbents in the context for PFAS remediation. Not only can they outperform commercial adsorbents such as GAC and anion exchange resins, but they also display rapid kinetics with equilibrium times under 1 min in some cases. However, their ability to assist in the context of real-world remediation is yet to be proven. The adsorption capacity will vary for different PFAS molecules, and some will be more effective with different chain lengths. In addition, the presence of co-contaminants should also be considered as well as the impact of ions and pH. Initial studies using water spiked with PFOA or PFOS as model PFAS are acceptable but should be followed up with tests of samples collected from contaminated sites.

Handling spent material is a common problem across all adsorbents. The ability to regenerate the MOF and recover PFAS for reuse would make these materials much more
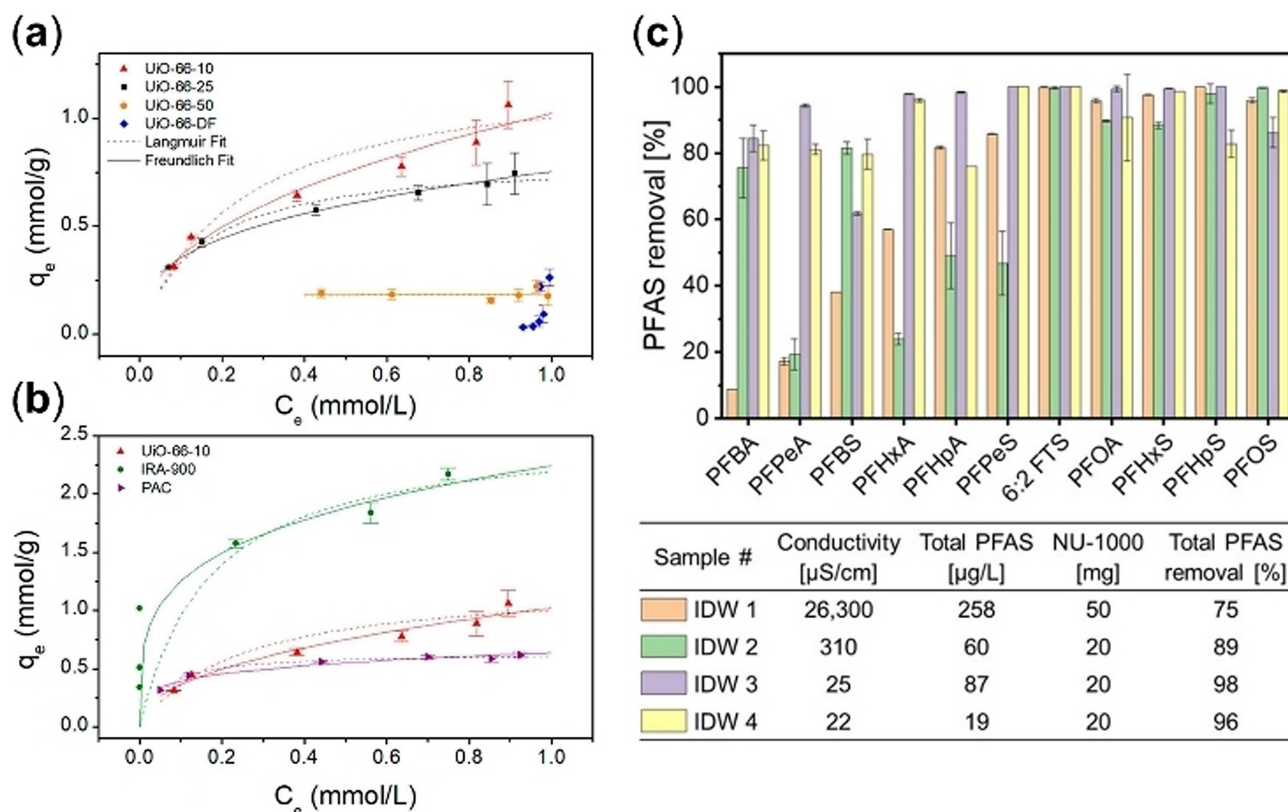
Figure 2. PFAS adsorption by MOFs. (a) Comparison of the UiO-66 materials with increasing engineered defects and (b) of UiO-66-10 to PAC and IRA900. The PFOS sorption isotherms at pH 5 were fitted with Langmuir and Freundlich isotherm models with the equilibrium PFOS concentration (C_e) in solution plotted against the equilibrium sorption amount of each sorbent (q_e). Adapted with permission from Ref. [20]. Copyright 2019, American Chemical Society. (c) Removal capacities of various PFAS from contaminated groundwater samples by the MOF NU-1000. Adapted with permission from Ref. [22]. Copyright 2021, American Chemical Society.

sustainable. While the studies discussed here often characterize the materials post-sorption, only two attempted to regenerate them. The regeneration conditions are relatively mild and quite efficient. Liu et al.[15] show overnight treatment of the MOF with 1% sodium chloride/methanol (30:70, v/v) allows for a 90% retention in adsorption capacity after three cycles. A more in-depth regeneration study was conducted by Li et al.,[22] where a number of inorganic salt and solvent combinations were tested. They identified 0.1 M hydrochloric acid in methanol (30:70, v/v) as optimal and were able to recover 86–105% of PFBS after 5 cycles. However, regeneration may not always be possible and PFAS often requires high-temperature incineration to be destroyed. Hence, technologies that can break down PFAS into safe constituents are of high demand.

3. Breakdown and Mineralization

An ideal technology for PFAS degradation should result in the generation of less harmful products such as complete mineralization to fluoride ions. As fluoride is a weak base, it mostly remains in ionic form in aqueous solutions; however, there is potential for the formation of the highly toxic and corrosive species hydrofluoric acid, which has been observed for some

remediation techniques.[27] Incomplete breakdown can also form short-chain PFAS, for which there are still questions regarding the safety of these molecules. While some of the following examples provide detailed mechanisms, which include the intermediates and products generated, it is not always provided and is something to remain mindful of when designing a remediation process.

3.1. Photocatalytic degradation

Harnessing the energy of photons from sunlight to destroy C—F bonds via photocatalysis is a green and cost-effective alternative to incineration. Photocatalysis involves the alteration of chemical reaction rates through photon absorption in the presence of a light-sensitive semiconductor (or photocatalyst). While mechanisms between individual systems may differ, the general process involves the following steps: (1) formation of electron-hole pairs following light absorption at an appropriate wavelength, (2) charge separation where the electron is excited to a higher state, (3) electron transfer to holes on the catalyst surface, and finally (4) a redox reaction using the formed charges (Figure 3a).[28] An analogous process occurs in photocatalytic MOFs where electrons are excited from the highest
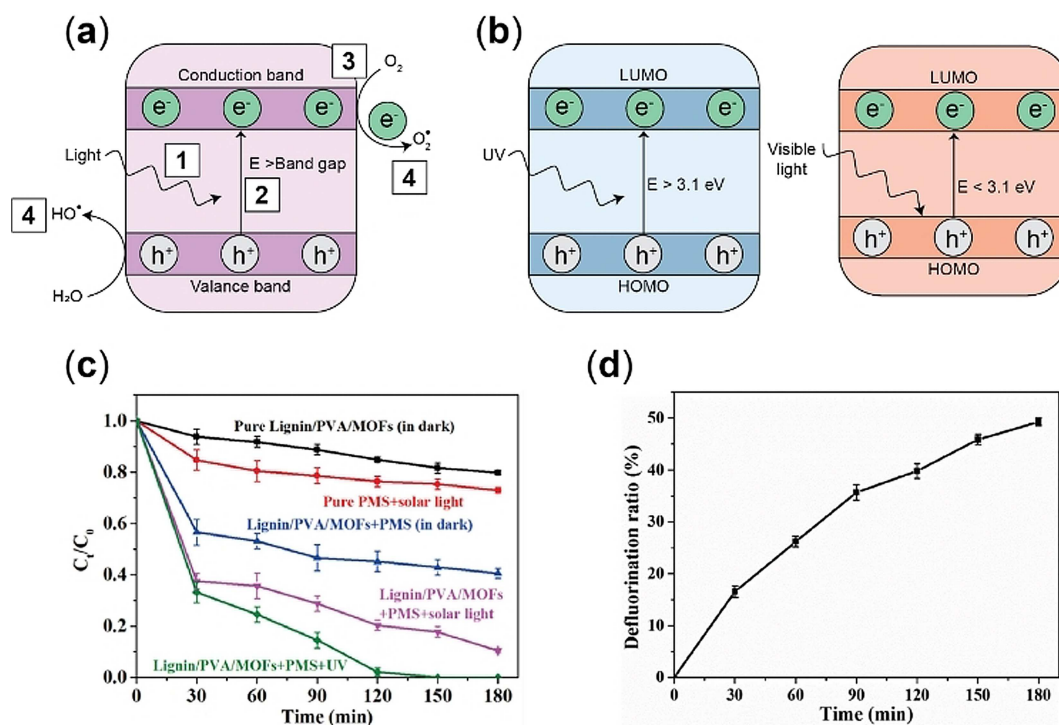
ChemSusChem

Review
doi.org/10.1002/cssc.202201136

**Chemistry
Europe**
European Chemical
Societies Publishing

Figure 3. (a) Conventional semiconductor photocatalysis, where electrons move from the valence to conduction band (examples include TiO_2 and ZnO), compared with (b) MOF photocatalysis, where the transition occurs from HOMO to LUMO, with comparison of bandgaps and light source. Adapted from Ref. [25] with permission from the Royal Society of Chemistry. (c) Photocatalytic degradation of PFOA by electrospun lignin-based bimetallic MOFs nanofibers composite membranes. Degradation of PFOA in the various composite membranes and (d) generation of fluoride in the peroxymonosulfate/membranes/solar light system over 180 min with a starting concentration of $20 \, mg \, L^{-1}$. Reprinted from Ref. [26], Copyright 2021, with permission from Elsevier.

occupied molecular orbital (HOMO) to the lowest unoccupied molecular orbital (LUMO) (Figure 3b).[28]

One of the main issues in photocatalysis is that charge carriers are vulnerable to fast recombination (at < 100 ns), which reduces the efficiency.[29] The photocatalyst should be easily modifiable to achieve an optimum bandgap and longer excitation lifetimes that can delay the electron–hole recombination to enhance the photocatalytic performance. As such, MOFs have recently gained attention for their ability to degrade a variety of organic pollutants by photocatalysis.[30] Photocatalytic MOFs are constructed from metal clusters that behave like inorganic photocatalysts and organic linkers that function as light-absorbing components (antenna). The porous structure of MOFs further allows their integration with chromophores or inorganic materials for improved performance. The high structural tunability of MOFs promotes the formation of narrower bandgaps that facilitate electronic excitation by visible light, thereby placing MOF photocatalysts in a favorable position for sunlight activation. The recombination of charge carriers can be inhibited to improve their photocatalytic performance through flexible structural modifications.[31] Hence, the combination of excellent adsorption capacities and photocatalytic properties offers the potential for accelerated degradation of organic wastes.[25,32] The collective desire by government agencies, chemical industries, and academia to eliminate the persistent and highly toxic PFAS from the environment has resulted in much research for ideal photocatalytic materials.[33–37]

Although MOF-based photocatalytic research for PFAS solutions is still in its infancy. Hou et al. recently fabricated lignin-based nanofiber (lignin/PVA/bi-MOFs) composite membranes that contain bimetallic Co/Fe MOFs for the photodegradation of PFOA in the presence of peroxymonosulfate as an advanced oxidizer, using sunlight irradiation.[26] The degradation process for PFOA is a combination of advanced oxidation processes and photocatalysis. The presence of the Co/Fe MOF increased the removal of PFOA from the solution through adsorption, generation of charge carriers and different reactive intermediates by the photoactivated Co/Fe MOF. About 90% PFOA was degraded under sunlight irradiation within 3 h while 100% degradation was achieved after 9 W UV irradiation at 185 nm, 5 cm above the solution (Figure 3c). This corresponded with defluorination and conversion to fluoride ions of approximately 50% (Figure 3d). The disparity between PFOA degradation and fluoride generation was attributed to adsorption of the ion to the catalyst surface and the generation of shorter-chain perfluorocarboxylates, which, as mentioned, may be just as problematic. This study demonstrates that the excellent adsorption property of MOFs combined with photocatalysis will promote their adoption as ideal materials for removal of PFAS from the environment.

ChemSusChem

Review
doi.org/10.1002/cssc.202201136

Chemistry
Europe
European Chemical
Societies Publishing

3.2. Enzymes and bacterial breakdown of PFAS

Bioremediation aims to remove pollutants from contaminated soil or water using microbes or their enzymes. It is seen as a green and economical alternative to other remediation techniques as they have evolved to carry out difficult reactions under environmentally friendly and low-cost conditions such as lower temperatures, atmospheric pressure, and using water as a solvent. As such, they have attracted attention as potential agents for degrading a wide range of xenobiotic compounds. At the time of writing, no singular enzyme has been identified that can directly degrade PFOA or PFOS. However, there is evidence microbes are able to break C–F bonds in partially fluorinated compounds[38,39] as well as some enzymes that can indirectly degrade PFAS through free-radical mediators. Furthermore, a bacterial strain (*Acidimicrobium* sp. Strain A6) was recently identified that is also able to degrade PFOA/PFOS.[40]

Bacteria carry an energy cost to maintain the organism, so using enzymes directly would be advantageous in this regard. The biotransformation of PFAS using enzymes with mediators is facilitated by an important class of reactions called enzyme-catalyzed oxidative humification reactions (ECOHRs), which are responsible for the decomposition of organic matter to produce the dark colored humus or compost in soils. These extracellular ligninolytic enzymes include lignin peroxidase (LnP, EC 1.11.1.14), manganese peroxidase (MnP, EC 1.11.1.13), horseradish peroxidase (HRP, EC 1.11.1.7), and phenol peroxidase (Laccase, E.C. 1.10.3.2). In nature, they use phenolic or anilinic moieties to produce free-radical intermediates. This allows them to degrade materials indirectly rather than directly through binding of the contaminant to the active site.

Early work on PFAS focused on the enzyme horseradish peroxidase (HRP). This metalloenzyme has a heme group at its active site that has been used extensively in the degradation of synthetic dyes containing phenolic groups.[41] Colosi et al. explored the degradation of PFOA using HRP, hydrogen peroxide, and a phenolic co-substrate (4-methoxyphenol), demonstrating approximately 68% depletion of the parent compound and 98% depletion of its related acute aquatic toxicity after 6 h.[42] However, there was less than 1% conversion to fluoride, and the enzyme mostly broke down the PFOA into smaller perfluorinated compounds. Laccase has also been considered in the breakdown of a variety of xenobiotic compounds. This enzyme contains a catalytic copper center, only requires oxygen as a reactant, and produces water as a product.[45] Their potential role in breaking down PFAS has been demonstrated by Huang and co-workers in two separate studies on PFOA and PFOS. They showed 50% of PFOA could be broken down over 157 days with 28% conversion to fluoride (Figure 4a)[43] while 59% of PFOS was over 162 days with 47% converted to fluoride (Figure 4b),[44] both using 1-hydroxybenzotriazole as a mediator and generating multiple small-chain fluorinated compounds. However, in both studies fresh enzyme and mediator was added every 6 days over the experimental time period. Even with additional enzyme, the breakdown does not appear to be linear. There may be several explanations such as the generation of unfavorable conditions (e.g., a change in pH or the production of side products) that inhibit further degradation.

These enzymes are known to be inactivated by the presence of different molecules. Peroxidases can be deactivated by hydrogen peroxide[46] and laccases by mediators[47] as well as products.[48] Immobilization of enzymes with MOFs has been shown extensively to protect enzymes under conditions that deviate from normal operating parameters including temperature and variations in pH.[49–56] Enzymes can be either immobilized onto the MOF surface or loaded into the MOF by infiltration within the limits of loading capacity of each of these techniques.[57–68] A more advanced technique is biomimetic mineralization,[69] wherein the MOF self-assembles around the enzyme (de novo encapsulation) and has been proven to significantly enhance stability (Figure 4c).[70] Negatively charged enzymes are postulated to increase the local concentration of the positively charged metal ions followed by an increase in organic ligands resulting in self-assembly. This leads to the facilitation of a prenucleation MOF cluster forming around these biomacromolecules which results in controlled crystal formation.[70,71] The overall process is uncomplicated and sustainable, requiring only ambient conditions and water-based synthesis, which can be easily scaled-up and translated to industrial production facilities. The intrinsic properties of the MOF materials including their high chemical, thermal, and mechanical stability are the main contributing factors to the resulting performance of the MOF–enzyme composites.[72] While the MOF scaffolds impart exceptional protection, their high porosity allows for access of the enzyme to reactants and products. The ability to structurally confine and stabilize enzymes using MOFs would allow for their continuous use for remediation in environmental conditions without the impracticality of supplementation.[73]

Laccase is amongst the multiple enzymes that have so far been incorporated with this technique in MOFs. Knedel et al. used the zeolitic imidazolate framework ZIF-8 to demonstrate improved thermal and chemical stability compared to free laccase.[74] They showed the free enzyme was completely inactivated after 5 h at 70°C while the ZIF-8-shielded enzyme retained 60% of its activity with the substrate 2,6-dimethoxyphenol as well as improved resistance to the solvent dimethylformamide. However, encapsulation hampered enzyme activity. Only 13% of the activity was retained when encapsulated compared to free enzyme.

Using the copper-trimesic acid MOF HKUST-1, Zhang et al. showed in addition to the increased thermal and chemical stability, the MOF in fact increased activity (1.5 fold) relative to the free enzyme.[79] They attributed this to a synergistic effect between the Cu^{2+} ions in HKUST-1 and the active site of laccase. In addition, the encapsulated enzyme had improved storage and retained around 70% activity after 30 days compared to laccase in solution. Finally, they demonstrated approximately 100% degradation of the pollutant bisphenol A within 4 h compared to around 35% for the free enzyme.

Using microorganisms to breakdown pollutants has also gained a lot of interest as a sustainable remediation approach; however, only a few have reported on the biodegradation of
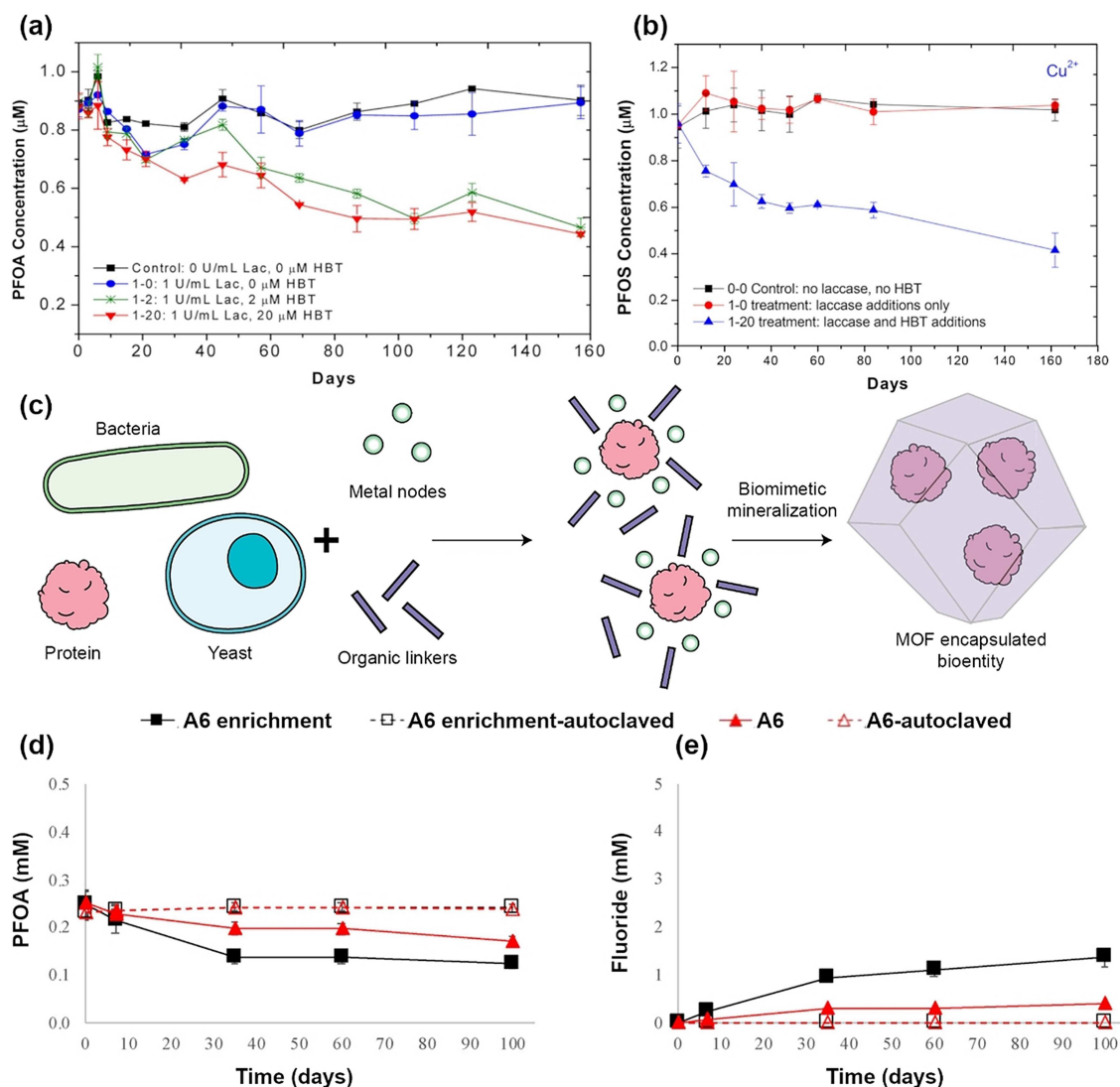
ChemSusChem

Review
doi.org/10.1002/cssc.202201136

Chemistry Europe
European Chemical
Societies Publishing

Figure 4. Enzyme-catalyzed degradation of PFAS, MOF encapsulation of bioentities, and bacterial breakdown. Change in (a) PFOA or (b) PFOS over time catalyzed by laccase with the mediator 1-hydroxybenzotriazole (HBT) with samples: 0 control, positive control sample with no laccase or HBT added; 1–0, 1 unit mL^{-1} laccase added every 6 days but no HBT; 1–2, 1 unit mL^{-1} laccase and 2 µM HBT added every 6 days; 1–20, 1 unit mL^{-1} laccase and 20 µM HBT added every 6 days. (a) Adapted with permission from Ref. [43]. Copyright 2015, American Chemical Society. (b) Adapted from Ref. [44]. Copyright 2018, American Chemical Society. (c) Biomimetic mineralization, wherein negatively charged bioentities increase the local concentration of the positively charged metal ions followed by an increase in organic ligands resulting in self-assembly of a MOF. (d) Reduction in PFOA from a starting concentration of 0.24 mM and (e) increase in fluoride when incubated with pure A6 and A6 enrichment bacterial cultures. Adapted with permission from Ref. [40]. Copyright 2015, American Chemical Society.

PFAS. It was shown that a *Pseudomonas parafulva* strain (YAB1) obtained near a PFAS producing facility showed 32% breakdown of PFOA over 96 h[80] while a *Pseudomonas aeruginosa* strain found in wastewater treatment sludge was able to remove 67% of PFOS of 48 h.[81] More recently, Huang and Jaffé reported on the ability of *Acidimicrobium* sp. strain A6 to breakdown both PFOA and PFOS by 60% over 100 days (Figure 4d) while also showing an increase in fluoride ions (Figure 4e).[40]

The chemical properties of PFAS contaminated soil and water are highly variable, so any bioremediation approach will require the microbes to survive under a range of conditions. As with enzymes, MOFs have been used to encapsulate living cells

for augmentation. Liang et al. demonstrated this on yeast cells (*Saccharomyces cerevisiae*) where they formed a ZIF-8 coating.[82] They demonstrated that this shield was able to enhance cell viability under extreme conditions where 70% of coated cells survived versus 1% unencapsulated cells after 7 days. The MOF-coated cells were also more resilient when subjected to UV radiation and cytotoxic compounds. In addition, the bacterial strain *Morella thermoacetica* was shielded using a zirconium and 1,3,5-benzenetribenzoate MOF.[83] This anaerobic bacteria is of interest for artificial photosynthesis and can suffer from a loss in viability due to oxygen and hydrogen peroxide at the cell membrane. By coating the cells in the MOF, the peroxide decomposed the zirconium oxide units, preventing the accumu-

ChemSusChem

Review
doi.org/10.1002/cssc.202201136

**Chemistry
Europe**
European Chemical
Societies Publishing

lation of reactive oxygen species and increasing viability 5-fold relative to uncoated cells.

While still in its infancy, it is clear MOFs have immense potential in fortifying enzymes, microorganisms and may do so for PFAS degrading entities as well. The porous MOF shell enables simultaneous access to the degradation target while shielding from chemical and physical assaults. In addition, their facile synthesis via biomimetic mineralization is carried out in water at room temperature. However, there are some challenges that must be overcome before MOFs can be implemented for remediation. Many metals and ligands that MOFs are composed of are toxic, especially to aquatic life (e.g., copper). However, there has been research into the synthesis of MOFs from edible components that may overcome this hurdle.[84] It is important to stress advances in this field hinge on the further identification and engineering of bioentities capable of efficiently breaking down PFAS. As there are currently limited examples in the literature, work in this area should be a priority to exploit the protective features of MOFs in the development of a sustainable bioremediation approach for PFAS.

4. Detection of PFAS using MOF Sensors

Chemical sensors can give real-time information about the identity and quantity of a specific analyte in a complex mixture. A good sensor should be sensitive, selective for the chemical of interest, as well as field-deployable for on-site detection.[85] A sensor contains materials that can chemically interact or physically adsorb the analyte to produce measurable physical signals. The development of chemical sensors for the detection of PFAS in water is challenging due to the limited chemistry of the molecules: the high C—F bond dissociation energy and weak non-polar interaction exhibited by perfluoroalkyl chains. Moreover, PFAS molecules have similar headgroups to most anionic surfactants, such as the linear alkylsulfonates and linear alkylcarboxylates, whose presence in water causes interference with the detection of PFAS due to their similar chemical interactions.[86]

MOFs are promising for chemical sensing due to their large surface areas, uniform pore structures for size-sieving of molecules, a wide range of metal clusters, and functionalizable organic linkers to provide tunable adsorption sites. MOFs consist of pores that can concentrate analytes to maximize interactions with the inorganic clusters, organic linkers, or both

simultaneously.[87] MOFs are potential candidates for the development of integrated sensing devices due to their flexible synthesis and modifiable properties. The use of MOFs for the detection of PFAS is a recent but promising development and showcases their capabilities at attaining high sensitivity and selectivity to different PFAS molecules through different sensing platforms.

A few studies have focused on PFAS sensing with MOFs and are summarized in Table 2, which includes the mode of interaction with PFAS in Figure 5a. Similar to studies on adsorption and breakdown, sensor development has mostly focused on the isolated detection of the most well-known PFAS molecules. Given the extensive and growing number of PFAS, future work in this area should focus on techniques that can identify total PFAS quantities and within complex mixtures.

4.1. Electrochemical detection of PFAS

Electrochemical sensing with MOFs requires that the electrical properties change in response to the adsorption of analytes. Cheng et al.[75] were the first to develop a MOF-based sensor for PFAS using MIL-101(Cr) to capture PFOS with electrochemical impedance spectroscopy (EIS) measurements. Their device consisted of interdigitated microelectrodes that are sandwiched with MIL-101 on microfluidic channels. The microfluidic electrochemical-MIL-101 (Cr) sensor attained a detection limit of $0.5 \, \text{ng L}^{-1}$ PFOS. MIL-101(Cr) is a mesoporous MOF that has strong affinity and high adsorption capacity for PFOS.[21] Upon exposure of MIL-101(Cr) to PFOS, a redox process occurs between the Cr^{III} site of the MIL-101, which is oxidized, and the C—F surface of the perfluoroalkyl, which is reduced. The high-resolution X-ray photoelectron spectroscopy (XPS) spectra of MIL-101 before and after adsorption of PFOS, showing the regions of F 1 s and $Cr \, 2p_{3/2}$, reveal that the intensity of the reduced F and oxidized Cr states increased after PFOS adsorption (Figure 5b). XPS also demonstrated a redox interaction between the Cr^{III} centers and the F atoms of PFOS. The shifting of spectra position of the $S \, 2p_{3/2}$ to a slightly lower binding energy indicates an electrostatic interaction between the Cr^{III} center and sulfonate head group of PFOS. Thus, the electrochemical impedance response of the sensor was enhanced by the stronger electrostatic interaction. The advantage of the MIL-101(Cr) electrochemical sensor is the linear dependence of the PFOS concentration on the charge transfer

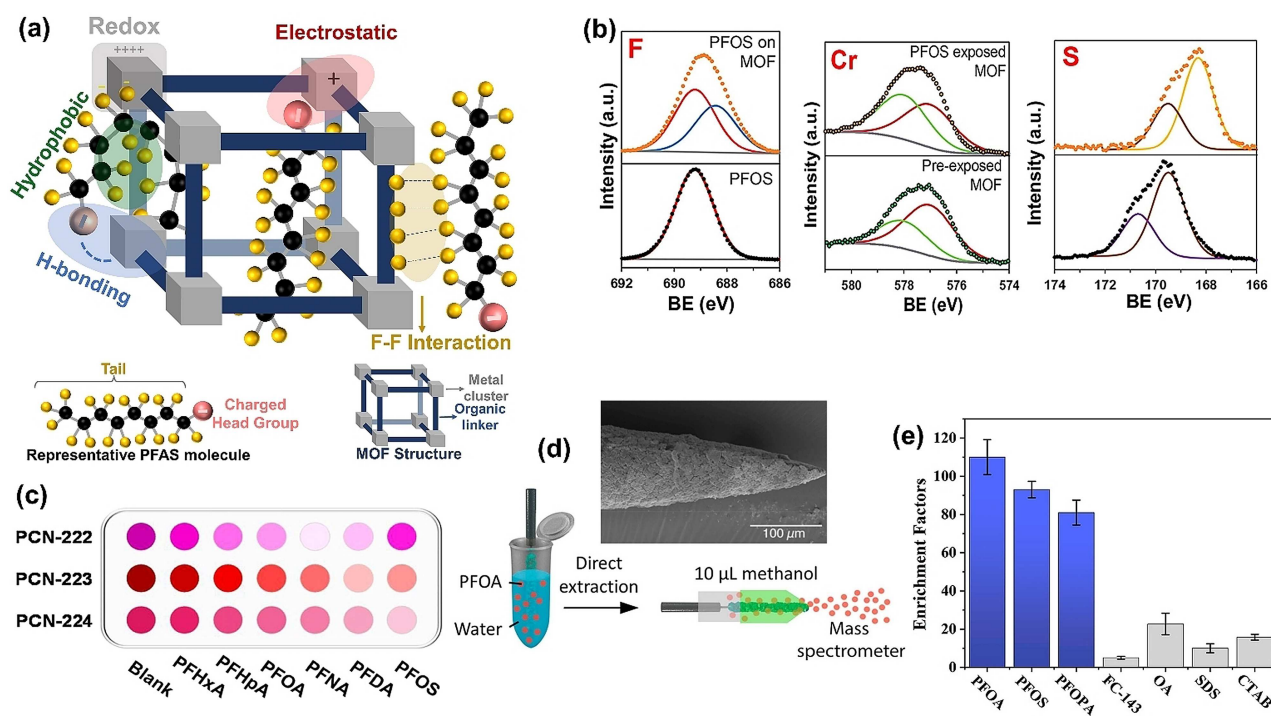| Table 2. MOF sensors for PFAS.						
MOF sensor	PFAS detected	Sensing platform	Limit of detection $[\text{ng L}^{-1}]$	Sensor preparation time	Analysis time	Ref.
Impedance Microfluidic MIL-101(Cr)	PFOS	electrochemical	0.5	not reported	2 h	[75]
PCN-222, PCN-223, PCN-224(Zr)Luminescent Sensor Array	PFHxA, PFHpA, PFOA, PFNA, PFDA, and PFOS	fluorescence	$3.6–4.7 \times 10^4$	not reported	10 s	[76]
ZIF-8-SPME probe	PFOA	SPME and MS	11	24 h	3 min	[77]
MIL-101(Cr)-DETA-F-SPME probe	PFOA, PFOS, and PFOPA	SPME and liquid chromatography–MS	0.004–0.12	≈4 h	15 min	[78]

ChemSusChem

Review
doi.org/10.1002/cssc.202201136

Chemistry Europe
European Chemical
Societies Publishing

Figure 5. (a) Schematic showing the different chemical interactions between MOF structures with PFAS molecules resulting in various chemical sensing responses. (b) High-resolution XPS of pristine PFOS and PFOS-exposed Cr-MIL-101 showing the (left) F 1s region, (middle) the Cr 3p$_{3/2}$ region of Cr-MIL-101, and (right) the S 3p region. Adapted with permission from Ref. [75]. Copyright 2020, American Chemical Society. (c) Fluorescence response patterns for different PFAS species using the luminescent PCN sensor array, adapted with permission from Ref. [76]. Copyright 2021, American Chemical Society. (d) Diagram of the PFOA sensing process using MOF-SPME probes. The probes were used to preconcentrate PFOA molecules from water samples and then desorbed in 10 μL methanol for mass spectrometry analysis; (top) cross-section SEM image of ZIF-8-SPME probe showing ZIF-8 particles grown on the surface of a polydopamine-coated stainless-steel needle, adapted with permission from Ref. [77]. Copyright 2020, American Chemical Society. (e) Enrichment factors of MIL-101-DETA-F for a mixture of seven compounds (1.0 μg L^{-1} for each). Reproduced with permission from Ref. [78]. Copyright 2021, American Chemical Society.

resistance of the device that allows the direct quantification of PFOS in water samples.

4.2. Fluorescent sensing of PFAS using a MOF sensor array

In a recent study performed by Chen et al., the promise of optical sensing of PFAS by a fluorescent MOF array was demonstrated.[76] The sensor array consisted of three zirconium-based porphyrinic coordination networks (PCNs (PCN-222, PCN-223, and PCN-224) to sense and discriminate different mixtures of PFAS in both surface and underground water samples. The MOF sensing array was used to distinguish between six different PFAS by producing a unique fluorescent response pattern for each species, depending on their adsorptive interaction with the MOFs. The six PFAS include: perfluorohexanoic acid (PFHxA), perfluoroheptanoic acid (PFHpA), perfluoroctanoic acid (PFOA), perfluorononanoic acid (PFNA), perfluorodecanoic acid (PFDA), and perfluorooctane sulfonate (PFOS). The main sensing mechanism reported is based on the adsorption of PFAS, which leads to the static quenching of the PCN fluorescence. Static quenching occurs due to the formation of stable non-fluorescent ground state complexes[88] and is different within the sensor array at the same concentration of PFAS (Figure 5c).

The various levels of quenching given by the sensor array after contact with PFAS molecules is due to the differences in the Zr-node connectivity, pore size, and surface areas of the Zr-PCN MOFs, which dictate their interactions with different PFAS molecules. The major interactions that are responsible for the various quenching responses observed include hydrophobic interactions between the aromatic pore walls and PFAS tail and electrostatic interactions between the positively charged Zr-clusters and the anionic heads of PFAS. The combination of these were leveraged to give significant quenching response to PFOS over other PFAS molecules due to stronger hydrophobic interactions with pore wall and electrostatic sulfonate head-group interaction with the Zr-clusters.

4.3. MOF-based solid phase microextraction detection of PFAS

The detection of PFAS with MOFs has further been demonstrated by leveraging their adsorptive properties through solid-phase microextraction (SPME). SPME is an analytical technique that uses adsorbent-coated fibers to extract target analytes from a solution phase. This process is usually combined with conventional analytical tools such as mass spectrometry (MS)

ChemSusChem

Review

doi.org/10.1002/cssc.202201136

**Chemistry
Europe**

European Chemical
Societies Publishing

and chromatography to desorb and quantify the analyte from the fiber.[89] Suwannakot et al. fabricated MOF-coated SPME probes that were combined with MS for the detection of PFOA based on four different MOFs [ZIF-8, MIL-88-A, UiO-66, and Tb$_2$(BDC)$_3$] (Figure 5d).[77] PFOA was adsorbed by the MOF-coated probe by dipping in water samples, followed by the desorption of PFOA from the probe in methanol for MS quantification. More PFOA is adsorbed on the surface of the probe as the specific surface area of the MOF increases. ZIF-8 and UiO-66 had higher abundance of PFOA than MIL-88-A and Tb$_2$(BDC)$_3$. Computational studies also revealed that both ZIF-8 and UiO-66 have the highest binding energy for PFOA. However, the ZIF-8-SPME probe gave more reproducible results and was therefore preferred over the UiO-66-SPME probe. The reported detection limit of ZIF-8-SPME probe for PFOA was 11 ng L^{-1}. The encouraging response of ZIF-8-SPME to PFOA may also be related to the strong hydrophobic interaction between the hydrophobic ZIF-8 surface[90] and perfluoroalkyl tail of PFOA.

One issue that needs consideration is how to minimize the interference of anionic surfactants in the MOF-based detection of PFAS. The hydrophobic interactions of the perfluoroalkyl tails of PFAS molecule with the organic walls of MOFs can be further exploited to improve their affinity over anionic surfactants with similar chemical structures. A window of opportunity, therefore, lies in the flexibility of MOFs for chemical functionalization. Jia et al.[78] used fluorinated diethylenetriamine (DETA)-functionalized MIL-101(Cr) (MIL-101-DETA-F) as a fiber coating for the SPME process that was combined with ultra-high-performance liquid chromatography-tandem MS to detect PFAS molecules. The MIL-101-DETA-F fiber demonstrated detection limits over the range of 0.004–0.12 ng L^{-1} to PFAS molecules. The enrichment factor (Figure 5e) indicates the difference in the abundance of each analyte to the MIL-101-DETA-F probe, and real water samples further showed that it was selective to PFOA, PFOS, and PFOPA molecules over non-fluorinated surfactants. The selectivity is due to the hydrophobic surface attracting only PFAS molecules through a non-polar F–F interaction of the functionalized MOF with the perfluoroalkyl tail. Other possible interactions include redox processes and hydrogen bonding between the parent framework and PFAS molecules.

MOF-based SPME sensing probes yield parts per trillion sensitivity, which is a function of the binding energy of PFAS with the MOF and the adsorption capacity. The large surface area and tunable surface chemistry of MOFs are needed to develop highly sensitive and selective probes. However, the dependence of the method on the bench-top analytical instruments for PFAS quantification is a drawback that limits its application for an on-site detection.

5. Summary and Outlook

As the evidence that per- and polyfluoroalkyl substances (PFAS) have negative impacts on health mounts, there is increasing pressure to remediate contaminated water and soil. Even though the use of these fluorinated compounds is tightly regulated now, the recalcitrant nature and historical widespread use means PFAS contamination is a problem that we will be facing for some time. Current methods for remediation of PFAS contaminated material are not sufficient, and better methods for detection are required. Metal-organic frameworks (MOFs) with their ultra-high surface area, tunable pore-size, and rich surface chemistries are proving extremely promising in addressing this issue. They are already demonstrating exceptional adsorption capacities for PFAS and the ability to degrade it through photocatalysis. In addition, they are highly effective at encapsulating and protecting bioentities and showing immense sensing capabilities. These properties make them a cost-effective and environmentally friendly approach for degrading PFAS.

However, much work still needs to be done before MOFs are used in the remediation of PFAS contamination. Firstly, the synthesis technique must be considered as many protocols require the use of harsh solvents and elevated temperatures, and hence, greener synthesis pathway should be investigated. Secondly, many MOFs are not aqueous-stable, which will need to be improved on for remediation and sensing applications. Thirdly, there are currently limited reports of either enzymes or bacteria that can degrade PFAS. However, many pollutants of concern that were previously thought to be completely resistant to biodegradation have later had enzymes identified that can in fact break them down.[91] Once identified, these enzymes can be subjected to directed evolution to improve their efficiency. Hence, synthetic biology together with advanced materials is likely to play a role in the future. If these challenges can be overcome, MOFs may prove extremely useful in multiple ways towards tackling the difficult problem that is PFAS contamination.

Conflict of Interest

The authors declare no conflict of interest.

[1] R. C. Buck, J. Franklin, U. Berger, J. M. Conder, I. T. Cousins, P. De Voogt, A. A. Jensen, K. Kannan, S. A. Mabury, S. P. J. van Leeuwen, *Integr. Environ. Assess. Manage.* **2011**, *7*, 513–541.

[2] J. N. Meegoda, J. A. Kewalramani, B. Li, R. W. Marsh, *Int. J. Environ. Res. Public Health* **2020**, *17*, 8117.

[3] D. O'hagan, *Chem. Soc. Rev.* **2008**, *37*, 308–319.

[4] B. C. Buer, J. L. Meagher, J. A. Stuckey, E. N. G. Marsh, *Proc. Natl. Acad. Sci. USA* **2012**, *109*, 4810–4815.

[5] S. E. Fenton, A. Ducatman, A. Boobis, J. C. DeWitt, C. Lau, C. Ng, J. S. Smith, S. M. Roberts, *Environ. Toxicol. Chem.* **2021**, *40*, 606–630.

ChemSusChem

Review

doi.org/10.1002/cssc.202201136

Chemistry
Europe

European Chemical
Societies Publishing

[6] S. Brendel, É. Fetter, C. Staude, L. Vierke, A. Biegel-Engler, *Environ. Sci. Eur.* **2018**, *30*, 9.

[7] I. Ross, J. McDonough, J. Miles, P. Storch, P. Thelakkat Kochunarayanan, E. Kalve, J. Hurst, S. S. Dasgupta, J. Burdick, *Remediation* **2018**, *28*, 101–126.

[8] S. T. M. L. D. Senevirathna, S. Tanaka, S. Fujii, C. Kunacheva, H. Harada, B. H. A. K. T. Ariyadasa, B. R. Shivakoti, *Desalination* **2010**, *260*, 29–33.

[9] E. W. Tow, M. S. Ersan, S. Kum, T. Lee, T. F. Speth, C. Owen, C. Bellona, M. N. Nadagouda, A. M. Mikelonis, P. Westerhoff, C. Mysore, V. S. Frenkel, V. Desilva, W. S. Walker, A. K. Safulko, D. A. Ladner, *AWWA Water Sci.* **2021**, *3*, 1–23. e1233.

[10] L. J. Winchell, J. J. Ross, M. J. M. Wells, X. Fonoll, J. W. Norton, K. Y. Bell, *Water Environ. Res.* **2021**, *93*, 826–843.

[11] Y. Wen, P. Zhang, V. K. Sharma, X. Ma, H. C. Zhou, *Cell Reports Phys. Sci.* **2021**, *2*, 100348.

[12] H.-C. Zhou, J. R. Long, O. M. Yaghi, *Chem. Rev.* **2012**, 673–674.

[13] P. S. Pauletto, T. J. Bandosz, *J. Hazard. Mater.* **2021**, 127810.

[14] N. C. Burtch, H. Jasuja, K. S. Walton, *Chem. Rev.* **2014**, *114*, 10575–10612.

[15] K. Liu, S. Zhang, X. Hu, K. Zhang, A. Roy, G. Yu, *Environ. Sci. Technol.* **2015**, *49*, 8657–8665.

[16] A. Cordner, V. Y. De La Rosa, L. A. Schaider, R. A. Rudel, L. Richter, P. Brown, *J. Exposure Sci. Environ. Epidemiol.* **2019**, *29*, 157–171.

[17] F. Wang, C. Liu, K. Shih, *Chemosphere* **2012**, *89*, 1009–1014.

[18] M. J. Chen, A. C. Yang, N. H. Wang, H. C. Chiu, Y. L. Li, D. Y. Kang, S. L. Lo, *Microporous Mesoporous Mater.* **2016**, *236*, 202–210.

[19] K. Sini, D. Bourgeois, M. Idouhar, M. Carboni, D. Meyer, *New J. Chem.* **2018**, *42*, 17889–17894.

[20] C. A. Clark, K. N. Heck, C. D. Powell, M. S. Wong, *ACS Sustainable Chem. Eng.* **2019**, *7*, 6619–6628.

[21] D. Barpaga, J. Zheng, K. S. Han, J. A. Soltis, V. Shutthanandan, S. Basuray, B. P. McGrail, S. Chatterjee, R. K. Motkuri, *Inorg. Chem.* **2019**, *58*, 8339–8346.

[22] R. Li, S. Alomari, R. Stanton, M. C. Wasson, T. Islamoglu, O. K. Farha, T. M. Holsen, S. M. Thagard, D. J. Trivedi, M. Wriedt, *Chem. Mater.* **2021**, *33*, 3276–3285.

[23] J. Winarta, B. Shan, S. M. Mcintyre, L. Ye, C. Wang, J. Liu, B. Mu, *Cryst. Growth Des.* **2020**, *20*, 1347–1362.

[24] O. K. Farha, A. Ö. Yazaydin, I. Eryazici, C. D. Malliakas, B. G. Hauser, M. G. Kanatzidis, S. T. Nguyen, R. Q. Snurr, J. T. Hupp, *Nat. Chem.* **2010**, *2*, 944–948.

[25] Q. Wang, Q. Gao, A. M. Al-Enizi, A. Nafady, S. Ma, *Inorg. Chem. Front.* **2020**, *7*, 300–339.

[26] C. Hou, W. Chen, L. Fu, S. Zhang, C. Liang, Y. Wang, *Int. J. Biol. Macromol.* **2021**, *174*, 319–329.

[27] S. Verma, R. S. Varma, M. N. Nadagouda, *Sci. Total Environ.* **2021**, *794*, 148987.

[28] S. Zhu, D. Wang, *Adv. Energy Mater.* **2017**, *7*, 1700841.

[29] M. R. Hoffmann, S. T. Martin, W. Choi, D. W. Bahnemann, *Chem. Rev.* **1995**, *95*, 69–96.

[30] Y. Wen, M. Feng, P. Zhang, H.-C. Zhou, V. K. Sharma, X. Ma, *ACS ES&T Eng.* **2021**, *1*, 804–826.

[31] A. S. Belousov, E. V. Suleimanov, *Green Chem.* **2021**, *23*, 6172–6204.

[32] J. L. Wang, C. Wang, W. Lin, *ACS Catal.* **2012**, *2*, 2630–2640.

[33] D. Lu, S. Sha, J. Luo, Z. Huang, X. Zhang Jackie, *J. Hazard. Mater.* **2020**, *386*, 121963.

[34] J. N. Kuhn, Y. O. Sokefun, *ChemistrySelect* **2021**, *6*, 5225–5240.

[35] B. Xu, M. B. Ahmed, J. L. Zhou, A. Altaee, M. Wu, G. Xu, *Chemosphere* **2017**, *189*, 717–729.

[36] S. S. R. K. C. Yamijala, R. Shinde, K. Hanasaki, Z. A. Ali, B. M. Wong, *J. Hazard. Mater.* **2022**, *423*, 127026.

[37] C. Xia, X. Lim, H. Yang, B. M. Goodson, J. Liu, *J. Water Process Eng.* **2022**, *46*, 102556.

[38] N. Tseng, N. Wang, B. Szostek, S. Mahendra, *Environ. Sci. Technol.* **2014**, *48*, 4012–4020.

[39] J. Liu, S. Mejia Avendaño, *Environ. Int.* **2013**, *61*, 98–114.

[40] S. Huang, P. R. Jaffé, *Environ. Sci. Technol.* 2019, 53, 11410–11419..

[41] F. W. Krainer, A. Glieder, *Appl. Microbiol. Biotechnol.* **2015**, *99*, 1611–1625.

[42] L. M. Colosi, R. A. Pinto, Q. Huang, W. J. Weber, *Environ. Toxicol. Chem.* **2009**, *28*, 264–271.

[43] Q. Luo, J. Lu, H. Zhang, Z. Wang, M. Feng, S. Y. D. Chiang, D. Woodward, Q. Huang, *Environ. Sci. Technol. Lett.* **2015**, *2*, 198–203.

[44] Q. Luo, X. Yan, J. Lu, Q. Huang, *Environ. Sci. Technol.* **2018**, *52*, 10617–10626.

[45] L. Arregui, M. Ayala, X. Gómez-Gil, G. Gutiérrez-Soto, C. E. Hernández-Luna, M. Herrera De Los Santos, L. Levin, A. Rojo-Domínguez, D. Romero-Martínez, M. C. N. Saparrat, M. A. Trujillo-Roldán, N. A. Valdez-Cruz, *Microb. Cell Fact.* **2019**, *18*, 200.

[46] B. Valderrama, M. Ayala, R. Vazquez-Duhalt, *Chem. Biol.* **2002**, *9*, 555–565.

[47] D. Ibarra, J. Romero, M. J. Martínez, A. T. Martínez, S. Camarero, *Enzyme Microb. Technol.* **2006**, *39*, 1319–1327.

[48] S. Dasgupta, K. E. Taylor, J. K. Bewtra, N. Biswas, *Water Environ. Res.* **2007**, *79*, 858–867.

[49] X. Wu, J. Ge, C. Yang, M. Hou, Z. Liu, *Chem. Commun.* **2015**, *51*, 13408–13411.

[50] S. S. Nadar, V. K. Rathod, *Int. J. Biol. Macromol.* **2017**, *95*, 511–519.

[51] H. He, H. Han, H. Shi, Y. Tian, F. Sun, Y. Song, Q. Li, G. Zhu, *ACS Appl. Mater. Interfaces* **2016**, *8*, 24517–24524.

[52] M. Salgaonkar, S. S. Nadar, V. K. Rathod, *J. Environ. Chem. Eng.* **2019**, *7*, 102969.

[53] W. H. Chen, M. Vázquez-González, A. Zoabi, R. Abu-Reziq, I. Willner, *Nat. Catal.* **2018**, *1*, 689–695.

[54] X. Li, D. Li, Y. Zhang, P. Lv, Q. Feng, Q. Wei, *Nano Energy* **2020**, *68*, 104308.

[55] X. Cheng, J. Zhou, J. Chen, Z. Xie, Q. Kuang, L. Zheng, *Nano Res.* **2019**, *12*, 3031–3036.

[56] R. Singh, M. Musameh, Y. Gao, B. Ozcelik, X. Mulet, C. M. Doherty, *J. Mater. Chem.* **2020**, *1*, 3777.

[57] P. Li, J. A. Modica, A. J. Howarth, E. L. Vargas, P. Z. Moghadam, R. Q. Snurr, M. Mrksich, J. T. Hupp, O. K. Farha, *Chem* **2016**, *1*, 154–169.

[58] T. J. Pisklak, M. Macías, D. H. Coutinho, R. S. Huang, K. J. Balkus, *Top. Catal.* **2006**, *38*, 269–278.

[59] Y. Cao, Z. Wu, T. Wang, Y. Xiao, Q. Huo, Y. Liu, *Dalton Trans.* **2016**, *45*, 6998–7003.

[60] S. Jung, Y. Kim, S. J. Kim, T. H. Kwon, S. Huh, S. Park, *Chem. Commun.* **2011**, *47*, 2904–2906.

[61] C. M. Doherty, G. Grenci, R. Riccò, J. I. Mardel, J. Reboul, S. Furukawa, S. Kitagawa, A. J. Hill, P. Falcaro, *Adv. Mater.* **2013**, *25*, 4701–4705.

[62] W. Xu, L. Jiao, H. Yan, Y. Wu, L. Chen, W. Gu, D. Du, Y. Lin, C. Zhu, *ACS Appl. Mater. Interfaces* **2019**, *11*, 22096–22101.

[63] W. Ma, Q. Jiang, P. Yu, L. Yang, L. Mao, *Anal. Chem.* **2013**, *85*, 7550–7557.

[64] V. Lykourinou, Y. Chen, X. Wang, L. Meng, T. Hoang, L. Ming, R. L. Musselman, S. Ma, *J. Am. Chem. Soc.* **2011**, *133*, 10382–10385.

[65] X. Liu, W. Qi, Y. Wang, R. Su, Z. He, *Nanoscale* **2017**, *9*, 17561–17570.

[66] D. Feng, T. F. Liu, J. Su, M. Bosch, Z. Wei, W. Wan, D. Yuan, Y. P. Chen, X. Wang, K. Wang, X. Lian, Z. Y. Gu, J. Park, X. Zou, H. C. Zhou, *Nat. Commun.* **2015**, *6*, 5979.

[67] P. Li, S. Y. Moon, M. A. Guelta, S. P. Harvey, J. T. Hupp, O. K. Farha, *J. Am. Chem. Soc.* **2016**, *138*, 8052–8055.

[68] P. Li, Q. Chen, T. C. Wang, N. A. Vermeulen, B. L. Mehdi, A. Dohnalkova, N. D. Browning, D. Shen, R. Anderson, D. A. Gómez-Gualdrón, F. M. Cetin, J. Jagiello, A. M. Asiri, J. F. Stoddart, O. K. Farha, *Chem* **2018**, *4*, 1022–1034.

[69] K. Liang, R. Ricco, C. M. Doherty, M. J. Styles, S. Bell, N. Kirby, S. Mudie, D. Haylock, A. J. Hill, C. J. Doonan, P. Falcaro, *Nat. Commun.* **2015**, *6*, 7240.

[70] K. Liang, R. Wang, M. Boutter, C. M. Doherty, X. Mulet, J. J. Richardson, *Chem. Commun.* **2017**, *53*, 1249–1252.

[71] N. K. Maddigan, A. Tarzia, D. M. Huang, C. J. Sumby, S. G. Bell, P. Falcaro, C. J. Doonan, *Chem. Sci.* **2018**, *9*, 4217–4223.

[72] A. J. Howarth, Y. Liu, P. Li, Z. Li, T. C. Wang, J. T. Hupp, O. K. Farha, *Nat. Rev. Mater.* **2016**, *1*, 15018.

[73] R. Singh, G. Souillard, L. Chassat, Y. Gao, X. Mulet, C. M. Doherty, *Adv. Sustainable Syst.* **2020**, *4*, 2000059.

[74] T. O. Knedel, E. Ricklefs, C. Schlüsener, V. B. Urlacher, C. Janiak, *ChemistryOpen* **2019**, *8*, 1337–1344.

[75] Y. H. Cheng, D. Barpaga, J. A. Soltis, V. Shutthanandan, R. Kargupta, K. S. Han, B. P. McGrail, R. K. Motkuri, S. Basuray, S. Chatterjee, *ACS Appl. Mater. Interfaces* **2020**, *12*, 10503–10514.

[76] B. Chen, Z. Yang, X. Qu, S. Zheng, D. Yin, H. Fu, *ACS Appl. Mater. Interfaces* **2021**, *13*, 47706–47716.

[77] P. Suwannakot, F. Lisi, E. Ahmed, K. Liang, R. Babarao, J. J. Gooding, W. A. Donald, *Anal. Chem.* **2020**, *92*, 6900–6908.

[78] Y. Jia, J. Qian, B. Pan, *Anal. Chem.* **2021**, *93*, 11116–11122.

[79] R. Zhang, L. Wang, J. Han, J. Wu, C. Li, L. Ni, Y. Wang, *J. Hazard. Mater.* **2020**, *383*, 121130.

[80] L. B. Yi, L. Y. Chai, Y. Xie, Q. J. Peng, Q. Z. Peng, *Genet. Mol. Res.* **2016**, *15*, 2.

[81] B. G. Kwon, H. J. Lim, S. H. Na, B. I. Choi, D. S. Shin, S. Y. Chung, *Chemosphere* **2014**, *109*, 221–225.

[82] K. Liang, J. J. Richardson, J. Cui, F. Caruso, C. J. Doonan, P. Falcaro, *Adv. Mater.* **2016**, *28*, 7910–7914.

[83] Z. Ji, H. Zhang, H. Liu, O. M. Yaghi, P. Yang, *Proc. Natl. Acad. Sci. USA* **2018**, *115*, 10582–10587.

[84] R. A. Smaldone, R. S. Forgan, H. Furukawa, J. J. Gassensmith, A. M. Z. Slawin, O. M. Yaghi, J. F. Stoddart, *Angew. Chem. Int. Ed.* **2010**, *49*, 8630–8634; *Angew. Chem.* **2010**, *122*, 8812–8816.

[85] O. S. Wolfbeis, *Angew. Chem. Int. Ed.* **2013**, *52*, 9864–9865; *Angew. Chem.* **2013**, *125*, 10048–10049.

[86] R. F. Menger, E. Funk, C. S. Henry, T. Borch, *Chem. Eng. J.* **2021**, *417*, 129133.

[87] L. E. Kreno, K. Leong, O. K. Farha, M. Allendorf, R. P. Van Duyne, J. T. Hupp, *Chem. Rev.* **2012**, *112*, 1105–1125.

[88] M. H. Gehlen, *J. Photochem. Photobiol. C* **2020**, *42*, 100338.

[89] N. Reyes-Garcés, E. Gionfriddo, G. A. Gómez-Ríos, M. N. Alam, E. Boyacl, B. Bojko, V. Singh, J. Grandy, J. Pawliszyn, *Anal. Chem.* **2018**, *90*, 302–360.

[90] A. U. Ortiz, A. P. Freitas, A. Boutin, A. H. Fuchs, F. X. Coudert, *Phys. Chem. Chem. Phys.* **2014**, *16*, 9940–9949.

[91] L. P. Wackett, S. L. Robinson, *Biochem. J.* **2020**, *477*, 2875–2891.